High-precision Monte Carlo study of the two-dimensional XY Villain model

Wolfhard Janke

Institut für Theoretische Physik, Freie Universität Berlin, Arnimallee 14, D-1000 Berlin 33, Germany
and Höchstleistungsrechenzentrum, Forschungszentrum Jülich, Postfach 1913, D-5170 Jülich, Germany

Klaus Nather

Institut für Theoretische Physik, Freie Universität Berlin, Arnimallee 14, D-1000 Berlin 33, Germany

We report two sets of high-precision Monte Carlo simulations of the two-dimensional XY model in Villain's formulation on large square lattices, employing the single-cluster update algorithm. In one set of simulations we use improved estimators to study the correlation length ξ and susceptibility χ in the high-temperature phase. On a 1200×1200 lattice this allows measurements up to $\xi \approx 140$ with statistical errors less than 0.25%. We judge quantitatively the advantage of using improved estimators, estimate autocorrelation times, and compare the numerical efficiency of various definitions of the correlation length. From least-square fits to these data we find clear support for the exponential divergence predicted by Kosterlitz and Thouless. The other set of simulations is performed in the vicinity of the transition point. Here we apply finite-size-scaling theory to obtain an estimate for the exponent η at criticality.

I. INTRODUCTION

According to a famous theorem by Mermin, Wagner, and Hohenberg,[1] two-dimensional (2D) statistical systems with short-range interactions and continuous symmetry cannot sustain long-range order for all nonzero temperatures. For $O(2)$ symmetric systems, however, early analyses[2] of high-temperature series expansions suggested some kind of phase transition. Motivated by this observation, Kosterlitz and Thouless (KT) (Refs. 3 and 4) developed a simple physical picture in terms of topological excitations and, on the basis of approximate renormalization-group calculations, predicted a peculiar phase transition governed by an essential singularity. Accordingly, if the critical temperature T_c is approached from high temperatures, the correlation length ξ and susceptibility χ should diverge *exponentially*,[4]

$$\xi \propto \exp(bt^{-\nu}), \quad \chi \propto x^{2-\eta}, \tag{1}$$

while the specific heat should stay finite at T_c. Here $t \equiv T/T_c - 1 > 0$ is the reduced temperature, $b \approx 1.5$ is a nonuniversal constant, and

$$\nu = \tfrac{1}{2}, \quad \eta = \tfrac{1}{4} \tag{2}$$

are universal critical exponents. In the physical picture underlying the KT theory, the transition is caused by the dissociation of vortex-antivortex pairs at T_c. Below the critical temperature, these pairs are tightly bound and merely renormalize the spin-wave excitations, which destroy long-range order down to zero temperature.[5]

Both the physical picture and the predictions (1) and (2) have been questioned many times.[6,7] Alternative considerations[7] favor *power-law* singularities of the form

$$\xi \propto t^{-\nu}, \quad \chi \propto t^{-\gamma}, \tag{3}$$

with conventional critical exponents ν and γ [$= \nu(2-\eta)$,

provided scaling is valid].

Besides a few magnetic systems,[8] the most important physical realization of such 2D $O(2)$ systems are layers of superconducting materials and films of liquid helium.[9] To clarify the nature of the phase transition in these systems is also of importance for a better understanding of Josephson-junction arrays.[10] Recently renewed interest has arisen in the context of high-T_c superconductivity.[11,12] It is currently believed that many properties can be modeled effectively by stacks of $O(2)$ symmetric layers with extremely weak intralayer couplings.[12] The associated crossover effects between two-dimensional and three-dimensional critical behavior turn out to be quite intricate.[13] Similar problems arise in studies[14] of stacks of two-dimensional layers of XY spins with isotropic couplings, where the addition of more and more layers causes a different type of crossover effect. It is therefore important to resolve first the discrepancies in the limiting two-dimensional case.

Recent studies in this direction employing high-temperature series expansions[15-17] and Monte Carlo (MC) simulations[18-22] are based on lattice models of the planar XY type with local spin-spin interactions taken in the so-called cosine form,

$$E = - \sum_{\mathbf{x},i} \vec{s}(\mathbf{x})\vec{s}(\mathbf{x}+i) = - \sum_{\mathbf{x},i} \cos[\nabla_i \theta(\mathbf{x})], \tag{4}$$

where $\vec{s} = (\cos\theta, \sin\theta)$ are unit spins, and $\nabla_i \theta(\mathbf{x}) \equiv \theta(\mathbf{x}+i) - \theta(\mathbf{x})$ are the lattice gradients in the i direction of a simple square lattice. Both approaches favor the KT scenario, but in particular the MC results are not completely conclusive.

The form of the energy (4) is motivated mainly by numerical convenience. Conceptually, however, it is not the simplest choice since it is well known that with this energy, vortex and spin-wave degrees of freedom are coupled in a complicated nonlinear way.[23] The KT arguments

and subsequent analyses[24,25] on the other hand assume (sometimes implicitly) that vortices and spin waves are decoupled. While universal properties should be insensitive to this assumption, it is conceivable that the quantitative approach of criticality does depend on the vortex spin-wave coupling. In order to investigate this issue it is therefore worthwhile to consider a related model in which vortices and spin waves are explicitly decoupled by construction, namely, the periodic Gaussian or Villain model.[26]

In this paper we shall discuss in some detail the results of our extensive Monte Carlo simulations of this model on simple square lattices of size $V = L \times L$ using the single-cluster update algorithm. More precisely we shall present high precision data from two sets of simulations: one in the high-temperature phase, and the other at criticality. The paper is organized as follows. In Sec. II, we first recall the periodic Gaussian model and its equivalent representations, and compile previous estimates of the critical parameters. Section III is devoted to a discussion of the observables we have measured and their theoretically expected properties. In Sec. IV we describe the set-up of our Monte Carlo simulations using the single-cluster update algorithm and low-variance estimators for correlation functions. The results of the first set of simulations in the high-temperature phase[27] are presented in Sec. V. In particular, we shall discuss several aspects concerning the single-cluster update procedure and low-variance estimators for correlation functions. Since we worked in quite an extreme regime with correlation lengths in the range $10 \leq \xi \leq 140$ on lattices with up to 1200×1200 sites, a thorough study of these points is important for a reliable simulation. In Sec. VI we discuss the results of our second set of simulations in the vicinity of the critical point and describe the finite-size-scaling analysis to estimate the exponent η. Finally, in Sec. VII we give a brief summary and discuss the main conclusions.

II. MODEL

The partition function of the periodic Gaussian or Villain model[26] is given by

$$Z = \prod_x \left[\int_{-\pi}^{\pi} \frac{d\theta(\mathbf{x})}{2\pi} \right]$$
$$\times \sum_{\{n_i(\mathbf{x})\}} \exp\left[-\frac{\beta}{2} \sum_{\mathbf{x},i} (\nabla_i \theta - 2\pi n_i)^2 \right], \quad (5)$$

where the integer variables $n_i(\mathbf{x})$ run from $-\infty$ to ∞, and $\beta \equiv 1/T$ is the inverse temperature. We always employ the periodic boundary condition. By a standard duality transformation[28] the partition function (5) can be shown to be equivalent to the discrete Gaussian (DG) model,

$$Z \propto Z_{DG} = \sum_{\{h\}} \exp\left[-\beta^{DG} \sum_{\mathbf{x},i} (\nabla_i h)^2 \right], \quad (6)$$

where $h(\mathbf{x})$ are integer valued height variables running from $-\infty$ to ∞ [with $h(0)$ fixed, say] and $\beta^{DG} = 1/2\beta$. A further transformation[28] reveals explicitly the excitations in (5),

$$Z \propto Z_{SW} Z_{vort}, \quad (7)$$

with Z_{SW} denoting the spin-wave part and Z_{vort} the Coulomb gas (CG) partition function

$$Z_{vort} = \sum_{\{m\}}' \exp\left[-4\pi^2 \beta \frac{1}{2} \sum_{\mathbf{x},\mathbf{x}'} m(\mathbf{x}) v(\mathbf{x}-\mathbf{x}') m(\mathbf{x}') \right]. \quad (8)$$

Here the integer variables $m(\mathbf{x})$ describe vortices of charge m at site $\mathbf{x}$, interacting via a long-range 2D (lattice) Coulomb potential

$$v(\mathbf{x}) = \int_{-\pi}^{\pi} \frac{d^2k}{(2\pi)^2} \frac{\exp(i\mathbf{k}\cdot\mathbf{x})-1}{\sum_{i=1}^{2} 2(1-\cos k_i)} \approx -\frac{1}{2\pi}\ln|\mathbf{x}| - c$$
$$(|\mathbf{x}| \gg 1), \quad (9)$$

with $c = (\gamma + \frac{3}{2}\ln 2)/2\pi \approx 0.2573$. The prime at the summation symbol in (8) indicates that only neutral configurations $\sum_{\mathbf{x}} m(\mathbf{x}) = 0$ are allowed.

Recall that most if not all theoretical investigations of the KT theory start from the latter representation (8). The standard renormalization-group (RG) result for the (nonuniversal) critical inverse temperature is the implicit relation[4,29]

$$\beta_c = 2/\pi + 4e^{-(\pi^2/2)\beta_c} \approx 0.740 \quad (RG). \quad (10)$$

A rigorous lower bound on β_c is[30]

$$\beta_c \geq \frac{1}{2\ln\mu} \geq \frac{1}{2\ln(2D-1)}, \quad (11)$$

where $\mu = 2.638\,158\,53(3)$ (Ref. 31) is the numerically determined effective coordination number of self-avoiding random walks on a two-dimensional $(D=2)$ simple square lattice. Inserting the numbers, this gives the numerical or rigorous bounds

$$\beta_c \geq 0.5154 \geq 0.4551, \quad (12)$$

which, however, turn out to be quite poor. Indeed, the estimate of β_c from simulations[32] of the CG representation invoking directly the vortices and their interactions agreed with the RG prediction (10). And a recent MC study[33] of the dual DG model gave $\beta_c^{DG} = 0.677 \pm 0.010$, which translates into a value

$$\beta_c = 0.739 \pm 0.011 \quad (DG\text{-}MC) \quad (13)$$

that is also surprisingly near to the RG estimate (10).

III. OBSERVABLES

A. Static observables

For the numerical simulations it is useful to write the partition function (5) as

$$Z = \prod_x \left[\int_{-\pi}^{\pi} \frac{d\theta(\mathbf{x})}{2\pi} \right] \sum_{\mathbf{x},i} B[\nabla_i \theta(\mathbf{x}),\beta], \quad (14)$$

with the local Boltzmann factors

$$B(\nabla_i\theta,\beta)\equiv\sum_{n=-\infty}^{\infty}\exp\left[-\frac{\beta}{2}(\nabla_i\theta-2\pi n)^2\right]$$

$$=\frac{1}{\sqrt{2\pi\beta}}\left[1+2\sum_{b=1}^{\infty}e^{-b^2/2\beta}\cos(b\nabla_i\theta)\right]\ . \quad (15)$$

The first representation converges rapidly for *large* β, while the second "dual" representation is best suited for *small* β.

Since the Boltzmann factors $B(\nabla_i\theta,\beta)$ in the Villain formulation take quite an unusual form, let us first briefly recall the definition of the sample estimators for the thermal observables. The internal energy (per site) is given by

$$e=-\frac{\partial}{\partial\beta}\ln Z/V=\langle u[\theta,\beta]\rangle\ , \quad (16)$$

where

$$u[\theta,\beta]\equiv-\frac{1}{V}\sum_{\mathbf{x},i}\frac{\partial}{\partial\beta}\ln B(\nabla_i\theta,\beta)\ , \quad (17)$$

and the angular brackets denote thermal averages with respect to the partition function (14). The specific heat (per site) follows from

$$c=\frac{\partial e}{\partial T}=-\beta^2\frac{\partial e}{\partial\beta}$$

$$=\beta^2\left[V(\langle u^2\rangle-\langle u\rangle^2)-\left\langle\frac{\partial u}{\partial\beta}\right\rangle\right]\ . \quad (18)$$

The unusual extra term $\langle\partial u/\partial\beta\rangle$ arises from the complicated β dependence of the Villain Boltzmann factors in (15).

The spin-spin correlation function is defined as usual by

$$G(\mathbf{x}-\mathbf{x}')=\langle\vec{s}(\mathbf{x})\cdot\vec{s}(\mathbf{x}')\rangle=\langle\cos(\theta-\theta')\rangle\ , \quad (19)$$

and its integral gives the susceptibility

$$\chi=\frac{1}{V}\sum_{\mathbf{x},\mathbf{x}'}G(\mathbf{x}-\mathbf{x}')$$

$$=\sum_{\mathbf{x}}G(\mathbf{x})=V\left\langle\left[\frac{1}{V}\sum_{\mathbf{x}}\vec{s}(\mathbf{x})\right]^2\right\rangle=V\langle\vec{m}^2\rangle\ , \quad (20)$$

where $\langle\vec{m}^2\rangle$ denotes the mean-squared magnetization. Recall that in the thermodynamic limit, due to the violent phase fluctuations in two dimensions, $\langle\vec{m}\rangle=0$ for all nonzero temperatures. On periodic lattices the correlation function can be decomposed into Fourier modes,

$$G(\mathbf{x}-\mathbf{x}')=\frac{1}{V}\sum_{n_1,n_2=0}^{L-1}\hat{G}(\mathbf{k})e^{i\mathbf{k}\cdot(\mathbf{x}-\mathbf{x}')}\ , \quad (21)$$

with $\mathbf{k}\equiv(2\pi/L)(n_1,n_2)$. In the high-temperature phase the amplitudes for long-wavelength modes are effectively given by

$$\hat{G}(\mathbf{k})=a\left[\sum_{i=1}^2 2(1-\cos k_i)+m^2\right]^{-1}\stackrel{|\mathbf{k}|\to 0}{\approx}a\frac{1}{\mathbf{k}^2+m^2}\ , \quad (22)$$

with β-dependent prefactor a and "mass" m. Since correspondingly for large distances $|\mathbf{x}|\gg 1$ (but $|\mathbf{x}|\ll L/2$ for finite periodic lattices)

$$G(\mathbf{x})\propto|\mathbf{x}|^{-1/2}e^{-m|\mathbf{x}|}\ \ (|\mathbf{x}|\gg 1)\ , \quad (23)$$

the inverse mass is identified as the correlation length $\xi\equiv 1/m$. In order to avoid the powerlike prefactor and to increase effectively the statistics we have actually measured a projected ("zero-momentum") correlation function defined by [$\mathbf{x}=(x,y)$]

$$g(x-x')=\frac{1}{L}\sum_{y,y'=1}^{L}G(\mathbf{x}-\mathbf{x}')$$

$$=L\left\langle\left[\frac{1}{L}\sum_{y=1}^L\vec{s}(x,y)\right]\cdot\left[\frac{1}{L}\sum_{y'=1}^L\vec{s}(x',y')\right]\right\rangle\ , \quad (24)$$

i.e., the correlations of "line-magnetizations" $(1/L)\sum_{y=1}^L\vec{s}(x,y)$ at x and x'. Notice that on periodic lattices

$$\chi=\tfrac{1}{2}g(0)+\sum_{i=1}^{L-1}g(i)+\tfrac{1}{2}g(L) \quad (25)$$

is given by the trapezoidal approximation to the area $\int_0^L dx\,g(x)$ under the projected correlation function $g(x)$. Applying the summations in (24) to the Fourier decomposition of $G(\mathbf{x}-\mathbf{x}')$, it is easy to see that

$$g(x-x')=a\frac{1}{L}\sum_{n_1=0}^{L-1}\frac{e^{ik_1(x-x')}}{2(1-\cos k_1)+m^2}\ . \quad (26)$$

This can be evaluated exactly as

$$g(x)=\frac{a}{2\sinh m^*}\frac{\cosh[m^*(L/2-x)]}{\sinh(m^*L/2)}\ , \quad (27)$$

with m and m^* related by

$$\frac{m}{2}=\sinh\left[\frac{m^*}{2}\right],\ \ \frac{m^*}{2}=\ln\left\{\frac{m}{2}+\left[\left[\frac{m}{2}\right]^2+1\right]^{1/2}\right\}\ . \quad (28)$$

For $\xi>10$ ($m<0.1$) the difference between ξ and $\xi^*\equiv 1/m^*$ is completely negligible, $(\xi^*-\xi)/\xi<0.042\%$. Notice that there is no x-dependent prefactor in (27).

Alternatively, one may also measure directly the Fourier amplitudes

$$\hat{G}(\mathbf{k})=\sum_{\mathbf{x}}G(\mathbf{x})e^{-i\mathbf{k}\cdot\mathbf{x}}=\frac{1}{V}\langle|\vec{s}(\mathbf{k})|^2\rangle\ , \quad (29)$$

for a few long-range modes $\vec{s}(\mathbf{k})=\sum_{\mathbf{x}}\vec{s}(\mathbf{x})e^{i\mathbf{k}\cdot\mathbf{x}}$. In the present work, we have used $\mathbf{k}=2\pi\mathbf{n}/L$ with $\mathbf{n}=(0,0)$, $(1,0)$, $(1,1)$, $(2,0)$, and $(2,1)$. Notice that in our normalization

$$\hat{G}(0) = \chi .\tag{30}$$

From (22) we know that

$$\hat{G}(\mathbf{k})^{-1} = \frac{1}{a}\left[\sum_{i=1}^{2} 2(1-\cos k_i) + m^2\right] \equiv c_1 \kappa^2 + c_0 ,\tag{31}$$

so that the squared correlation length

$$\xi^2 = 1/m^2 = c_1/c_0 \tag{32}$$

can be extracted from linear fits of $\hat{G}(\mathbf{k})^{-1}$ versus $\kappa^2 = \sum_{i=1}^{2} 2(1-\cos k_i) \approx \mathbf{k}^2$. Note that this method gives directly ξ (and not ξ^*).

B. Dynamic observables

In order to investigate the performance of the single-cluster update algorithm for the 2D Villain model and to get reliable error estimates on equilibrium measurements, we have also recorded the (normalized) autocorrelation functions

$$A(k) = \frac{\langle O_i O_{i+k}\rangle - \langle O_i\rangle^2}{\langle O_i^2\rangle - \langle O_i\rangle^2} ,\tag{33}$$

where O_i stands for the ith measurement of the energy, the correlation function, or the susceptibility. Typically, for large k, $A(k)$ decays exponentially,

$$A(k) \propto \exp(-k/\tau_0) .\tag{34}$$

This defines the exponential autocorrelation time τ_0. As far as equilibrium properties are concerned, the integrated autocorrelation time

$$\tau = \frac{1}{2} + \sum_{k=1}^{\infty} A(k) \tag{35}$$

is of greater importance. It enters directly in the error estimate ϵ for the mean of N correlated measurements with variance σ^2,

$$\epsilon = \left[\frac{2\tau}{N}\sigma^2\right]^{1/2} \equiv \left[\frac{\sigma^2}{N_{\text{eff}}}\right]^{1/2} .\tag{36}$$

Here $N_{\text{eff}} \equiv N/2\tau \leq N$ is a measure for the effective statistics of an equivalent, uncorrelated sample. In practice the estimates of $A(k)$ for large k are very noisy and the infinite summation in (35) must be cut off at some finite $k = k_{\max}$. In our simulations we have used a self-consistent windowing procedure with $k_{\max} \approx 6\tau$. Errors on τ can be estimated by the usual binning procedure or, if more accuracy is required, by the jackknife method. A useful *a priori* estimate is[34]

$$\epsilon_\tau = \left[\frac{2(2k_{\max}+1)}{N}\right]^{1/2}\tau \approx \left[\frac{12}{N_{\text{eff}}}\right]^{1/2}\tau ,\tag{37}$$

implying that already for a 5% accuracy we would need a statistics of $N_{\text{eff}} \approx 5000$ or $N \approx 10\,000\tau$ measurements.

IV. SIMULATION

A. Update algorithm

To update the angles $\theta(\mathbf{x})$ we have used the cluster algorithm[35] in its single-cluster (1C) (Ref. 36) variant. For the cosine model it has been demonstrated that with this algorithm critical slowing down is dramatically reduced in 2D (Ref. 19) and 3D (Ref. 37). Recall that one 1C update step consists of (i) choosing a random mirror line with normal $\vec{r}$, and (ii) a random site $\mathbf{x}_0$, being the starting point for (iii) growing a cluster of reflected spins. In the cosine model (4) the last step is governed by the probability for activated links

$$P_A = 1 - \min(1, \exp\{\beta[R\vec{s}(\mathbf{x})\cdot\vec{s}(\mathbf{y}) - \vec{s}(\mathbf{x})\cdot\vec{s}(\mathbf{y})]\}) ,\tag{38}$$

where $\mathbf{x}$ and y are nearest neighbors, and

$$R\vec{s}(\mathbf{x}) = \vec{s}(\mathbf{x}) - 2\vec{r}[\vec{r}\cdot\vec{s}(\mathbf{x})] \tag{39}$$

describes the reflection of $\vec{s}(\mathbf{x})$ on the mirror line orthogonal to $\vec{r}$. In order to adapt this procedure to the Villain model we parametrize $\vec{s} = (\cos\theta, \sin\theta)$ and $\vec{r} = (\cos\phi, \sin\phi)$. Then, for the cosine model with Boltzmann factors $B(\nabla_i\theta, \beta) = \exp[\beta\cos(\nabla_i\theta)]$, (38) and (39) may be written equivalently as

$$P_A = 1 - \min\{1, B[R\theta(\mathbf{x}) - \theta(\mathbf{y}), \beta]/B[\theta(\mathbf{x}) - \theta(\mathbf{y}), \beta]\} ,\tag{40}$$

with

$$R\theta(\mathbf{x}) = 2\phi + \pi - \theta(\mathbf{x}) .\tag{41}$$

But now it is obvious how (38) can be generalized to the Villain model. Simply insert in (40) the Boltzmann factors from (15). The update procedure is illustrated in Fig. 1, where we show a section around $\mathbf{x}_0$ of a 200×200 lattice with all spins rotated (globally) in such a way that $\vec{r}$ points in the x direction. The mirror line then runs in the y direction and the spins inside the cluster are reflected as indicated in the schematic drawing. This snapshot was taken during the simulations at $\beta = 0.59$ where $\xi \approx 11$. A few more typical clusters found in our simulations at $\beta = 0.59$ are shown in Fig. 2.

The evaluation of (15) is of course much more time consuming than the corresponding expression for the cosine model [which is actually best handled in the Cartesian representation of $\vec{s}(\mathbf{x})$]. We have first tried to minimize the computing time by expressing the cosines in (15) in terms of Chebyshev polynomials $\cos(b\nabla_i\theta) = T_b(\cos\nabla_i\theta)$. Apart from the prefactor, the second line in (15) then becomes a polynomial in $z = \cos\nabla_i\theta$, which can be evaluated quite efficiently. Still, the performance was not very satisfactory and consequently we finally decided to use the Z_N approximation (with $N = 100$) of the $O(2)$ symmetry. This approximation is known to be very accurate and allows the use of tables for $B(\nabla_i\theta, \beta)$, calculated once at the beginning of each run for fixed β. To implement it in the cluster algorithm, one only has to make sure that the mirror lines are restricted to appropriate angles. If $\theta = (2\pi/N)n$, $n = 0, \ldots, N-1$, then
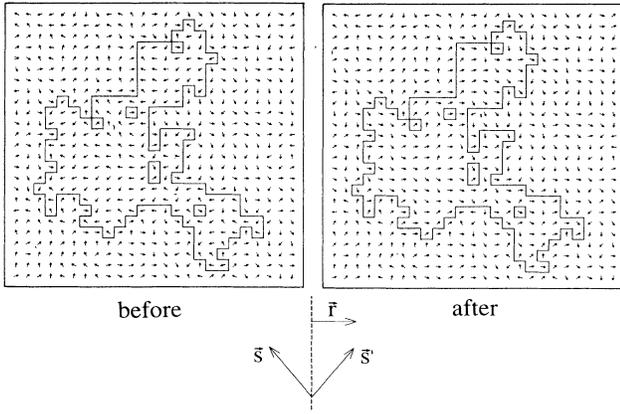
FIG. 1. Illustration of the single-cluster update. The mirror line is parallel to the y axis.

$\phi = (\pi/N)n, n = 0, \ldots, 2N-1$. Compared to typical update times for the Metropolis algorithm (on vector computers), the performance of the cluster update is nevertheless quite modest. To update one spin (not counting the measurements) our program needs around $6-7$ μsec on a CRAY-X MP. This low speed is of course more than compensated by the drastical reduction of critical slowing down near criticality.

B. Low-variance estimator for correlation function

In the high-temperature phase the performance of the simulation can further be improved by using low-variance estimators for the spin-spin correlation function. For the 1C algorithm they are given by[38]

$$\tilde{G} = 2\frac{V}{C}\vec{r}\cdot\vec{s}(\mathbf{x})\vec{r}\cdot\vec{s}(\mathbf{x}')\Theta_c(\mathbf{x})\Theta_c(\mathbf{x}') , \tag{42}$$
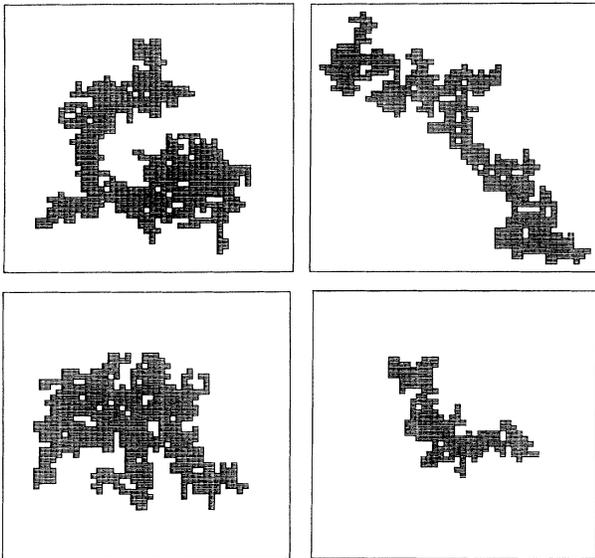
FIG. 2. A few typical clusters found in the simulation at $\beta = 0.59$ ($\xi \approx 11$) on a 200×200 lattice. Only the relevant section of the lattice is shown.

where $\vec{r}$ is the random unit vector used in the construction of the cluster $\mathcal{C}$ of reflected spins, C is the size or weight of the cluster, and $\Theta_c(\mathbf{x})$ denotes its characteristic function ($=1$ if $\mathbf{x}\in\mathcal{C}$ and 0 otherwise). The factor 2 accounts for the $O(2)$ symmetry. It has been demonstrated[38] that $\langle\tilde{G}\rangle = G$, and argued [or verified numerically for the 2D $O(3)$ model[38]] that averages over many cluster steps, $G_{\mathrm{imp}} \equiv (1/N_c)\sum_{n=1}^{N_c}\tilde{G}_n$, have much smaller variances than the conventional estimator in (19). Performing the summations in (24) we find the improved estimator for the projected correlation function $g(x-x')$, and from (29) we get for the Fourier amplitudes

$$\tilde{G}(\mathbf{k}) = \frac{2}{C}\left|\sum_{\mathbf{x}\in\mathcal{C}}\vec{r}\cdot\vec{s}(\mathbf{x})e^{-i\mathbf{k}\mathbf{x}}\right|^2$$

$$= \frac{2}{C}\left[\left[\sum_{\mathbf{x}\in\mathcal{C}}\vec{r}\cdot\vec{s}(\mathbf{x})\cos\mathbf{k}\mathbf{x}\right]^2 + \left[\sum_{\mathbf{x}\in\mathcal{C}}\vec{r}\cdot\vec{s}(\mathbf{x})\sin\mathbf{k}\mathbf{x}\right]^2\right] . \tag{43}$$

Putting $\mathbf{k}=0$ we finally obtain an improved estimator for the susceptibility,

$$\tilde{\chi} = 2C\left[\frac{1}{C}\sum_{\mathbf{x}\in\mathcal{C}}\vec{r}\cdot\vec{s}(\mathbf{x})\right]^2 . \tag{44}$$

Below we shall present quantitative comparisons of the conventional and improved observables.

These arguments remain valid for the Z_N approximation if one keeps the trivial single-site clusters [generated for $\vec{r}\bot\vec{s}(\mathbf{x}_0)$]. Alternatively, since trivial single-site clusters only replicate the old configurations in a uniform way, one may avoid them by a suitable prescription in the update procedure. Then the factor 2 has to be replaced by $2-2/N$. This gives a smooth interpolation between the Ising [$Z_2 = O(1)$] and XY [$Z_\infty = O(2)$] models. A useful check of these relations is provided by the identity

$$1 = 2\left\langle\frac{1}{C}\sum_{\mathbf{x}\in\mathcal{C}}[\vec{r}\cdot\vec{s}(\mathbf{x})]^2\right\rangle , \tag{45}$$

which follows by putting $\mathbf{x}=\mathbf{x}'$ in (42) and summing over $\mathbf{x}$.

V. RESULTS IN THE HIGH-T PHASE

A. Primary data

The first set of simulations was performed in the high-temperature phase. As primary observables we have chosen the correlation length and susceptibility since these observables are best suited to distinguish between the KT and a pure power-law scenario when approaching the critical point. The data for $\xi > 10$ are summarized in Tables I and II. The statistics is given in units of Metropolis sweeps, $t_{\mathrm{run}} = $ number of simulated clusters $\times\langle C\rangle/V$, where $\langle C\rangle$ is the average cluster size. This can be read off from Table II, where we give the ratio $\langle C\rangle/\chi_{\mathrm{imp}}$, which depends only very weakly on temperature and approaches $\langle C\rangle/\chi_{\mathrm{imp}} \approx 0.8105$ for $\xi > 40$, as expected from simulations of the cosine model.[19] We have

TABLE I. Correlation length data in the high-temperature phase. The run time is given in units of Metropolis sweeps, t_{run} = number of simulated clusters $\times \langle C \rangle / V$, and $f \times V$ is the average number of updated spins between measurements of the conventional estimators.

β	L	L/ξ_{imp}	$t_{run}/10^3$	f	ξ	ξ_{imp}	$\xi_{\widehat{G}}^{(5)}$
0.590	200	17.81	39.58	0.2452		11.231(16)	11.2270(78)
0.595	200	16.24	69.63	0.2694		12.313(10)	12.2960(67)
0.600	200	14.74	39.01	0.2478		13.567(19)	13.551(12)
0.605	200	13.34	73.61	0.2703		14.991(14)	14.9650(93)
0.610	200	12.03	88.72	0.2455		16.625(15)	16.598(11)
0.615	200	10.76	76.68	0.2711		18.591(20)	18.540(14)
0.620	200	9.60	89.06	0.2477		20.831(22)	20.801(16)
0.625	400	16.98	19.51	0.2422	23.30(18)	23.563(37)	23.551(23)
0.630	400	14.92	15.14	0.2543		26.812(50)	26.800(32)
0.635	400	12.99	21.27	0.2470	30.74(26)	30.786(52)	30.738(35)
0.640	400	11.22	21.72	0.2462		35.638(65)	35.565(44)
0.645	400	9.62	26.27	0.2446		41.597(81)	41.501(55)
0.650	400	8.14	34.93	0.2363	49.21(31)	49.160(88)	
0.655	600	10.23	21.00	0.2512	58.88(47)	58.68(12)	58.561(84)
0.660	600	8.45	21.51	0.2452	71.06(57)	70.97(15)	
0.665	800	9.15	24.93	0.2514	88.07(65)	87.42(17)	87.20(13)
0.670	800	7.28	35.50	0.2478	110.53(65)	109.91(21)	109.16(16)
0.675	1200	8.57	19.37	0.2450	140.44(74)	139.96(30)	139.61(23)

adjusted the run time to make sure that the errors on ξ_{imp} and χ_{imp} are always less than 0.25%. We have performed a "simulation of our simulation" to convince ourselves that by imposing this condition it is very improbable to misinterpret a true exponential behavior as a power law by chance. The opposite question is clearly not meaningful since the power law is a special limiting case of the exponential ansatz. In general such simulated simulations provide a very simple means to plan the numerical experiment. The improved observables were measured for each cluster, while measurements of the conventional observables were taken only after every mth cluster update step, with m chosen such that, on the average, $f \times V$ spins are updated between measurements. Since even for $f < 1$ the autocorrelation times are very small we have

chosen $f \approx 0.25$. Note that by choosing f still smaller, i.e., by performing more (weakly correlated) measurements, the errors on the conventional observables could be somewhat reduced. We did not try, however, to optimize our simulations in this direction. In Table II we also give the energy and specific heat which stays finite in the transition region and does not exhibit any peculiar behavior at β_c. This is expected for a KT-like transition. It is also known that the specific heat develops a smooth peak displaced from the transition point to higher temperatures. From further data for $\xi < 10$ on 100×100 lattices we have located the peak maximum at

$$\beta_{C_v,max} = 0.5387 \pm 0.0019 \tag{46}$$

with

TABLE II. Susceptibility, average cluster size, integrated autocorrelation time (in units of Metropolis sweeps), energy, and specific heat (from energy fluctuations) in the high-temperature phase.

β	L	χ	χ_{imp}	$\langle C \rangle / \chi_{imp}$	τ_χ	e	C_v
0.590	200	177.61(52)	177.74(17)	0.811 544	0.168(2)	1.107 86(10)	1.509(12)
0.595	200	207.56(48)	207.49(16)	0.811 415	0.179(2)	1.086 860(78)	1.4993(89)
0.600	200	243.32(71)	244.36(27)	0.811 261	0.171(2)	1.066 205(97)	1.423(12)
0.605	200	290.05(64)	289.82(26)	0.811 126	0.179(2)	1.046 191(74)	1.4630(90)
0.610	200	345.24(69)	345.94(31)	0.811 045	0.178(2)	1.026 672(64)	1.4212(77)
0.615	200	417.68(93)	417.93(44)	0.810 937	0.194(2)	1.007 961(72)	1.4218(85)
0.620	200	509.5(1.1)	509.21(56)	0.810 858	0.193(2)	0.989 510(64)	1.3838(74)
0.625	400	625.7(2.5)	628.78(84)	0.810 773	0.158(3)	0.971 911(70)	1.316(17)
0.630	400	777.8(3.5)	784.2(1.4)	0.810 678	0.159(3)	0.954 809(80)	1.398(20)
0.635	400	993.7(4.1)	995.1(1.7)	0.810 644	0.164(3)	0.938 444(67)	1.298(18)
0.640	400	1283.4(5.0)	1278.9(2.4)	0.810 603	0.177(3)	0.922 491(61)	1.268(13)
0.645	400	1655.3(6.1)	1665.2(3.3)	0.810 572	0.182(3)	0.907 356(57)	1.271(14)
0.650	400	2218.3(7.3)	2221.8(4.4)	0.810 536	0.206(3)	0.892 728(50)	1.189(13)
0.655	600	3019(13)	3015.6(6.4)	0.810 514	0.180(3)	0.878 688(41)	1.135(16)
0.660	600	4191(17)	4190(10)	0.810 488	0.187(3)	0.865 348(42)	1.167(16)
0.665	800	6018(23)	6015(13)	0.810 479	0.181(3)	0.852 488(31)	1.124(15)
0.670	800	8902(30)	8896(20)	0.810 457	0.206(3)	0.840 189(24)	1.073(12)
0.675	1200	13 594(58)	13 604(33)	0.810 457	0.182(3)	0.828 488(20)	1.034(16)

$$C_{v,\text{max}} = 1.5587 \pm 0.0028 . \tag{47}$$

The correlation length at this temperature is

$$\xi(\beta_{C_v,\text{max}}) = 5.33 \pm 0.05 . \tag{48}$$

For a graphical comparison of the specific heat computed from the energy fluctuations and by numerical differentiation of the energy, see Fig. 3.

In the following we shall comment in some detail on how the correlation length is measured and describe some of the consistency checks we have performed. The correlation length was determined from least-square fits to the right-hand side of (27), i.e., by fitting the data to

$$g(x) = \text{const} \times \cosh[(L/2 - x)/\xi^*] . \tag{49}$$

Since for small x also higher excitations are expected to contribute, we have used in these fits only data for $x > x_{\text{min}} \approx \xi$. For the improved correlation function on the 1200×1200 lattice (with $\xi \approx 140$) the quality of the fit can be inspected in Fig. 4.

We have checked in two ways that the choice $x_{\text{min}} \approx \xi$ gives reliable results. First, we have varied the cut by discarding all data points with $x < 2\xi$ and $x < 3\xi$, respectively. As a result we find only small and unsystematic differences which are completely covered by the error bars. Since the errors trivially increase with increasing x_{min} (by, e.g., a factor of about 1.3 for $x_{\text{min}} \approx 2\xi$), all ξ's quoted in Table I are from fits with $x_{\text{min}} \approx \xi$. Second, since for $x \ll L/2$, $g(x) \propto e^{-x/\xi}$, one can also plot the effective correlation length

$$\xi_{\text{eff}} \equiv 1/\ln[g(x)/g(x+1)] \approx \xi \tag{50}$$

versus x, and inspect visually where the plateau $\xi_{\text{eff}} = \text{const} = \xi$ sets in. For an illustration see Fig. 5. Clearly, for $L/2 - x \approx \xi$ also the (exactly known) finite-L corrections are seen in such a plot. As a rough estimate, the plateaus are thus expected in a range $\xi < x < L/2 - \xi$.

As another independent check on systematic errors of this fitting procedure we have measured in most cases also the improved estimators (43) of the Fourier ampli-

FIG. 4. Improved correlation function on the 1200×1200 lattice at $\beta = 0.675$ ($\xi \approx 140$). In (a) the difference between the data and the hyperbolic cosine fit is hardly visible. The relative deviations are shown in the much more sensitive plot (b).

tudes $\hat{G}(\mathbf{k})$ and calculated ξ from fits to (31), always using $\kappa^2 \equiv \sum_{i=1}^{2} 2(1 - \cos k_i)$ as an independent variable. By monitoring the goodness-of-fit parameter we concluded that using the small $|\mathbf{k}|$ approximation $\kappa \approx \mathbf{k}^2$ is usually not acceptable. In Table I these estimates are denoted by $\xi_{\hat{G}}^{(5)}$, indicating the number of long-range Fourier modes taken into account in the fits [$\mathbf{k}L/2\pi = (0,0)$, $(1,0)$, $(1,1)$, $(2,0)$, and $(2,1)$]. Our estimates based on $\xi_{\hat{G}}^{(4)}$ are almost identical.

For all temperatures the four estimates for ξ are consistent within their statistical errors. We observe, however, that the fits to the Fourier amplitudes systematically lead to somewhat smaller values than the fits to $g(x)$. This is particularly pronounced for $\beta = 0.670$ where the ratio $L/\xi \approx 7.3$ is smallest. In order to get quantitative information on how large this ratio should be for a reli-

FIG. 3. Specific heat in the high-temperature phase calculated from the energy fluctuations ($\bigcirc$) and by numerical differentiation ($\times$). Its broad peak is displaced from $\beta_c \approx 0.75$ to smaller β (higher temperatures) by about 25–30%. At β_c we find $C_v \approx 0.74$ (see Table VI).
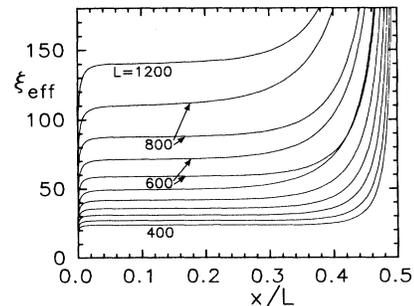
FIG. 5. Effective correlation length defined in Eq. (50) vs x/L.

able simulation, we have performed detailed finite-size-scaling analyses at $\beta = 0.55$ (where $\xi \approx 6$) and $\beta = 0.63$ (where $\xi \approx 27$). In these runs the ratio L/ξ was varied between 4 and 20. The resulting data for the correlation length, the susceptibility, and the specific heat (computed from the energy fluctuations) are compiled in Table III. The corresponding plots of $\xi_{imp}(L)$, $\xi_{\hat{G}}^{(n)}(L)$, $n = 2,3,4,5$, and $\chi_{imp}(L)$ versus L/ξ_∞ (ξ_∞ denotes the infinite volume limit) in Figs. 6 and 7 clearly show a saturation around $L/\xi \approx 8$. For the usually used lattice sizes $L \approx 6\xi$, the data are systematically lower, but this should only be important in very-high-precision studies with relative errors around 0.1%. We also see that for the definition of ξ based on $\hat{G}(\mathbf{k})$ the finite-size effects are more severe. On the other hand the statistical errors are somewhat smaller than for ξ_{imp}. Notice that even the simplest estimator $\xi_{\hat{G}}^{(2)} = \{\chi/\hat{G}[(1,0)] - 1\}^{1/2}/2\sin(\pi/L)$ (there is no fit involved) may be used. Of all $\xi_{\hat{G}}^{(n)}$ this has the smallest systematic corrections but the largest statistical errors which, however, are still comparable with those of ξ_{imp}. As a conclusion of this finite-size-scaling study we can recommend the use of the numerically very convenient momentum space definition of ξ as long as the lattices can be made large enough (compared to the correlation length). In our study we have chosen the lattice sizes to satisfy $L > 8\xi$ (apart from the one exception at $\beta = 0.67$ with $L \approx 7.3\xi$), which, in view of Figs. 6 and 7, seems to be a very safe condition.

After this discussion of possible systematic errors a few words are in order concerning the statistical errors. We have estimated them by the usual binning procedure, e.g., for the correlation length, by decomposing the whole run into large nonoverlapping blocks of many measurements, performing the fits to the block averages, and computing the variance of the fitted parameters. In most cases we have also recorded the time history of the runs (at least of the block averages) to make sure that only equilibrium configurations are used for the measurements. We have explicitly checked that using the cluster algorithm, the

equilibration from completely ordered or random initial configurations is extremely fast, i.e., the relaxation time is very short.

Once in equilibrium also the autocorrelation times turn out to be very small as expected from studies of the cosine model.[19] As can be read off from Table II, the integrated autocorrelation time τ_χ of the (conventional) susceptibility in units of Metropolis sweeps is around 0.2. For the energy we obtain in the same units $\tau_e \approx 3$. As far as CPU time is concerned this time scale (all directly measured times are rescaled by the factor $f \equiv$ number of cluster steps $\times \langle C \rangle /V$) is the proper way to compare the performance of the single-cluster update with other update algorithms. Compared with the correlation time of the Metropolis algorithm $\tau \propto \xi^z$ with $z \approx 2$ we find a tremendous saving in computing time. To achieve the same accuracy with the Metropolis algorithm for our largest correlation length $\xi \approx 140$, one would need roughly $140^2/0.2 \times 1/10 \approx 10\,000$ times more CPU time on a vector computer. (The factor $\frac{1}{10}$ roughly accounts for the fact that only part of the cluster algorithm was vectorized. For a workstation the same comparison is of course even more impressive.)

Finally recall that if only improved observables are measured, the computing time needed to achieve a given accuracy is independent of the lattice size L. Only the equilibration overhead, which clearly scales with the volume, and of course memory limitations prevent us from using even larger lattices. Analyzing the errors on our data for χ_{imp} we obtain the estimated CPU time $= (\xi/r)^2 (0.092 \pm 0.012) \times 10^6 t_0$, where r is the desired relative error of χ_{imp} in percent and $t_0 \approx 7$ μsec is the average time needed to update a single spin in our implementation of the single-cluster algorithm. In Fig. 8 it is demonstrated that for the susceptibility the ratio of statistical errors $\epsilon_{\chi_{imp}}/\epsilon_\chi$ scales with L/ξ_∞, where ξ_∞ is the infinite volume limit of the correlation length. And it indicates that for $L < \xi_\infty$ (i.e., deep in the finite-size-scaling

TABLE III. Lattice-size dependence of correlation length, susceptibility, average cluster size, and specific heat at $\beta = 0.55$ and 0.63. The run time t_{run} is given in units comparable to Metropolis sweeps.

L	$t_{run}/10^3$	ξ_{imp}	$\xi_{\hat{G}}^{(5)}$	χ_{imp}	$\langle C \rangle /\chi_{imp}$	C_v
			$\beta = 0.55$			
24	1175.5	5.9421(37)	5.8574(33)	59.128(39)	0.813 732	1.6297(25)
36	852.9	6.0463(32)	6.0062(25)	62.256(37)	0.813 594	1.5704(27)
48	513.6	6.0660(34)	6.0343(24)	62.718(37)	0.813 530	1.5655(36)
60	276.5	6.0596(39)	6.0415(26)	62.752(40)	0.813 534	1.5662(49)
72	184.73	6.0551(42)	6.0378(27)	62.660(40)	0.813 571	1.5498(58)
84	152.07	6.0646(40)	6.0463(26)	62.733(38)	0.813 498	1.5576(64)
120	189.21	6.0618(49)	6.0501(18)	62.773(24)	0.813 516	1.5573(56)

L	$t_{run}/10^3$	ξ_{imp}	$\xi_{\hat{G}}^{(5)}$	χ_{imp}	$\langle C \rangle /\chi_{imp}$	C_v
			$\beta = 0.63$			
160	126.83	26.789(33)	26.651(27)	782.53(1.11)	0.810 692	1.3299(59)
190	75.70	26.817(37)	26.667(28)	783.50(1.24)	0.810 709	1.3375(80)
220	112.78	26.839(29)	26.737(22)	784.30(0.91)	0.810 711	1.3222(73)
270	62.85	26.855(33)	26.780(23)	784.85(0.99)	0.810 715	1.3423(99)
400	15.14	26.812(50)	26.800(32)	784.22(1.33)	0.810 678	1.3981(198)
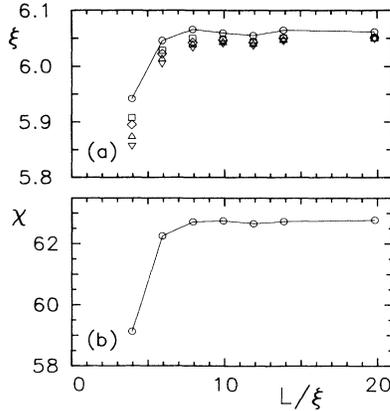
FIG. 6. Lattice-size dependence of (a) the correlation length and (b) the susceptibility at $\beta=0.55$ ($\xi\approx6$). Shown are the improved observables ($\bigcirc$), and in (a) for comparison also $\xi_G^{(2)}$ ($\square$), $\xi_G^{(3)}$ ($\lozenge$), $\xi_G^{(4)}$ ($\triangle$), and $\xi_G^{(5)}$ (∇).

region) the improved estimators are no longer advantageous. In Fig. 9 we compare the relative errors for the correlation function on the 1200×1200 lattice. We see that the improvement is most dramatic at large distances where the ratio of relative errors may, depending on L/ξ, exceed a factor of 10 (being equivalent to a factor of 100 in computing time).

As a final test of our computer programs we have also run a few simulations for the cosine model (4), where comparative data using different update algorithms were available.[18-21] Our results for relatively large correlation lengths are collected in Table IV. Our data are compatible with Wolff's[19] early simulations, using also the single-cluster algorithm but still standard observables, and with the recent study by Gupta and Baillie[21] employing both overrelaxation techniques and cluster updates. Note the greater accuracy of our correlation length data, which is mainly due to the use of improved estimators.

B. KT versus power-law fits of ξ and χ

In the final analysis we focused on the question of whether our data for ξ and χ in Tables I and II support a
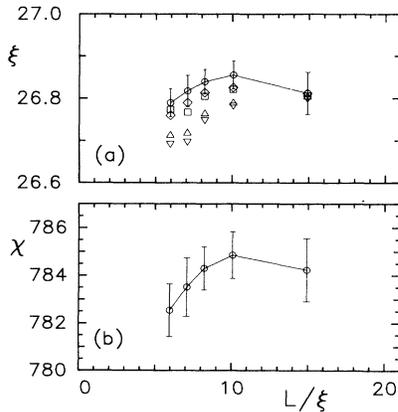
FIG. 7. Lattice-size dependence of (a) the correlation length and (b) the susceptibility at $\beta=0.63$ ($\xi\approx27$). The symbols have the same meaning as in Fig. 6.
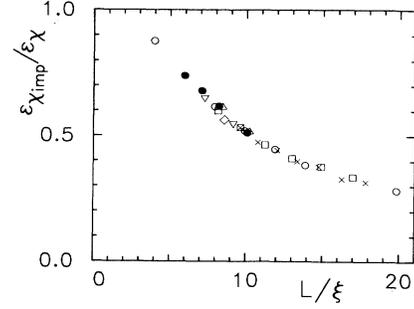
FIG. 8. Ratio of statistical errors of the improved and conventional estimators for the susceptibility, showing a pronounced scaling behavior with L/ξ. Shown are the data in Table II for $L=200$ ($\times$), 400 ($\square$), 600 ($\triangle$), 800 (∇), and 1200 ($\lozenge$), as well as the data in Table III at $\beta=0.55$ ($\bigcirc$) and 0.63 ($\bullet$).

KT transition governed by an exponential divergence (1) or a conventional transition with a power-law singularity (3). In order to decide between the two alternatives, we have performed χ^2 fits to ξ_{imp} and χ_{imp}. To be precise, we have fitted our 18 data points to the logarithms of the hypotheses (1) or (3),

$$\ln\xi(T)=A+b(T/T_c-1)^{-\nu} \quad (\text{KT}) ,\qquad(51)$$

or

$$\ln\xi(T)=A-\nu\ln(T/T_c-1) \quad (\text{power}) ,\qquad(52)$$

with similar expressions for χ. Furthermore, we can rewrite these expressions also as functions of β. Near T_c, in leading order, this amounts to replacing T/T_c-1 by $1-\beta/\beta_c$ in (51) and (52). The importance of correction terms omitted in (51) and (52), however, can be quite different for the T- and β-dependent ansatz.

The three-parameter power-law fits turned out to be very stable and different fit routines gave almost identical results. For the KT fits, however, the situation is much more complicated and requires some care. Keeping all four parameters in various standard nonlinear fit routines, we obtained quite inconsistent minima. At first sight this is surprising since the almost elliptic contour lines of constant χ^2 shown in Fig. 10 do not give any hints for the existence of various relative minima. But the parameters are so strongly intercorrelated that there
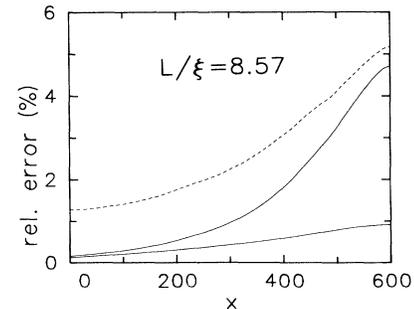
FIG. 9. Comparison of relative errors in measurements of the projected correlation function on the 1200×1200 lattice using conventional and improved estimators. The dashed line shows the ratio of these errors.

TABLE IV. Results for the cosine model in the high-temperature phase. The notations are the same as in Tables I and II.

β	L	L/ξ_{imp}	$t_{run}/10^3$	f	ξ	ξ_{imp}	$\xi_G^{(4)}$	$\xi_G^{(5)}$
0.97	256	11.80	33.07	0.2478	21.47(15)	21.688(34)	21.618(24)	21.606(24)
1.00	512	12.74	29.51	0.2493	40.22(29)	40.176(59)	40.110(43)	40.109(42)
1.02	512	7.35	44.54	0.2446	70.21(37)	69.69(12)	69.251(95)	69.224(93)
β	L	χ		χ_{imp}	$\langle C \rangle/\chi_{imp}$	τ_χ	e	C_v
0.97	256	553.7(1.9)		556.44(90)	0.810864	0.180(3)	$-1.273\,937(68)$	1.483(18)
1.00	512	1616.2(5.6)		1612.3(2.5)	0.810590	0.169(3)	$-1.318\,217(35)$	1.406(18)
1.02	512	4179(13)		4163.6(8.4)	0.810491	0.216(3)	$-1.345\,222(28)$	1.367(14)

is an extremely long and narrow valley in the χ^2 landscape. Once near the ground of this valley, the minimization algorithm has to determine its exact direction in the four-dimensional parameter space to proceed. This is obviously a very hard task. One way out of this problem is to observe that the parameters A and b enter in a linear way and may thus be determined exactly for any given pair of β_c and ν. In this way the problem reduces to a nonlinear two-parameter fit, which is much easier to perform. Using this procedure the fit routines gave the same minimum no matter from where we started.[39]

To compute error estimates on the fitted parameters, we have tried two different methods. First, using the already determined optimal parameter values as initialization of standard fit routines,[40] it is easy to get error estimates from the (approximate) covariance matrix computed from the curvature at the minimum. Although already this simple method gave quite reliable error estimates, we finally relied on a purely numerical approach,[40] in which the errors are estimated by drawing synthetic input data sets from Gaussian distributions with the measured variances, performing the fits, and cal-

FIG. 10. Confidence regions in the β_c-ν plane for the KT fits to the correlation length and susceptibility data. Shown are the contour lines for $\Delta\chi^2 \equiv \chi^2 - \chi^2_{min} = 1$, 2.30, 4.61, and 9.21. For a linear fit model and normally distributed errors, the projection of the $\Delta\chi^2 = 1$ region onto the axes gives the 68.3% confidence interval for a single parameter without regard to the other, while the other three regions are the 68.3%, 90% and 99% confidence intervals for β_c and ν jointly (Ref. 40). For the nonlinear KT fits this interpretation is only approximately valid.

culating the variance of the fitted parameters. In this way one can also check that the contour lines of constant χ^2 have indeed the correct probability interpretation. All errors quoted in Table V are determined by the latter procedure.

Our results in Table V clearly show that the pure power-law hypothesis can be ruled out with high confidence. Even the "best" $\chi^2 \approx 66$ for the $\xi(\beta)$ power-law fit corresponds to an extremely small goodness-of-fit parameter $Q \approx 2 \times 10^{-8}$. Recall that this is the probability to find a set of simulation data with $\chi^2 > 66$ by chance fluctuations, assuming that the power-law hypothesis is correct. This statistical "uncertainty principle" is why we have formulated our conclusion somewhat carefully—but nobody will really believe that we have picked such an unlikely event just by chance. This conclusion is in qualitative agreement with MC simulations of the cosine model. Quantitatively, however, the currently available evidence against the power-law hypothesis is much weaker [$Q \approx 2 \times 10^{-3}$ for $\chi(\beta)$ (Ref. 19)] for the cosine model.

All unconstrained KT fits, on the other hand, look equally consistent with a χ^2 around 10 corresponding to $Q \approx 0.8$. The quality of the fits can be inspected in Fig. 11. Since in a simple $\ln\xi$ (or $\ln\chi$) versus β plot all four fits look like an interpolation of the data and can hardly be distinguished, we have used the β-dependent KT fit as a reference line. It is remarkable that even on this very fine scale (the y axis corresponds to a maximal deviation of $\pm 1\%$ from the reference line) the two KT fits are practically indistinguishable over the whole data range. Notice that in evaluating the fits it is not sufficient to simply insert the rounded values of the fit parameters (with the significant digits determined by their *individual* error bars) as given in Table V. Due to the strong mutual correlations of the parameters (see Fig. 10) it is necessary to use much higher precision values.

We may thus conclude that of the two alternatives, a pure power-law or a KT divergence, we obtain unambiguous support for a KT-like transition in the 2D Villain model. It should be stressed again, however, that by statistical means it is in principle impossible to prove a given hypothesis in a strict sense. As a simple counterexample we have considered for the susceptibility a *generalized* power-law ansatz with additional confluent corrections of the type $\chi = at^{-\gamma} + bt^{-\gamma'}$ with $t \equiv 1 - \beta/\beta_c$, thereby introducing two further parameters. This yields good

TABLE V. χ^2 fits of the data for the correlation length ξ and susceptibility χ to the KT and power-law hypotheses (51) and (52). The arguments of ξ and χ indicate the specific form of the ansatz, and Q is the standard goodness-of-fit parameter. DOF indicates degrees of freedom.

Fit	χ^2	Q	A	b	β_c	ν
		Unconstrained	KT fits (14 DOF)			
$\xi(T)$	9.41	0.80	$-1.89(37)$	2.18(31)	0.7539(49)	0.532(55)
$\xi(\beta)$	9.68	0.79	$-5.5(1.4)$	4.6(1.3)	0.7466(53)	0.353(68)
$\chi(T)$	10.05	0.76	$-1.53(29)$	3.19(24)	0.7566(28)	0.588(32)
$\chi(\beta)$	9.81	0.78	$-6.32(90)$	6.00(81)	0.7497(31)	0.421(40)
		Constrained KT fits:	$\nu = \frac{1}{2}$ (15 DOF)			
$\xi(T)$	9.79	0.83	$-2.117(15)$	2.370(11)	0.751 06(36)	0.5
$\xi(\beta)$	13.87	0.54	$-3.551(24)$	2.812(14)	0.758 14(40)	0.5
$\chi(T)$	18.82	0.22	$-2.460(14)$	3.964(10)	0.748 90(20)	0.5
$\chi(\beta)$	13.39	0.57	$-4.855(22)$	4.702(13)	0.755 91(23)	0.5
		Power-law	fits (15 DOF)			
$\xi(T)$	257.20	4×10^{-46}	$-0.5749(54)$		0.710 69(20)	1.8818(50)
$\xi(\beta)$	65.96	2×10^{-8}	$-1.638(11)$		0.719 15(26)	2.3610(79)
$\chi(T)$	942.74	2×10^{-191}	0.1174(50)		0.708 89(11)	3.1533(46)
$\chi(\beta)$	250.33	1×10^{-44}	$-1.6638(94)$		0.717 23(14)	3.9543(73)

fits also, $\chi=0.0223(28)t^{-5.115(41)}+0.508(69)t^{-3.01(13)}$ at $\beta_c=0.73$ with $Q=0.82$, albeit with unreasonably large correction terms which make this ansatz unacceptable on general grounds.

The estimates for β_c from the unconstrained fits are quite consistent with an overall mean of

$$\beta_c=0.752\pm0.005 . \tag{53}$$

Recent simulations[41] of the dual discrete Gaussian model (6) (using the "mountain-valley reflection" cluster update and renormalization-group matching ideas) gave $\beta_c^{DG}=0.6645\pm0.0006$. This translates into $\beta_c=1/2\beta_c^{DG}=0.7524\pm0.0007$, in good agreement with (53).

The estimates for ν, however, show a systematic dependence on the form of the ansatz: the T-dependent fits give significantly larger values than the β-dependent fits. Correspondingly we observe that the confidence regions in the β_c-ν plane shown in Fig. 10 do not overlap. For the other two parameters A,b this discrepancy is even more pronounced. Unfortunately, since the χ^2 are almost equal for all KT fits, we have no numerical clue to decide which one is the best. This point is visually supported in Fig. 11 where the two KT fits for ξ (or χ) are hardly distinguishable over the whole data range. Taking the average as best estimate, we get

$$\nu=0.48\pm0.10 , \tag{54}$$

where the (rough) error estimate accounts for the systematic shifts. Although this value is in fairly good agreement with the KT prediction, this certainly cannot be considered as a stringent confirmation. To test this prediction more directly, we have also performed con-
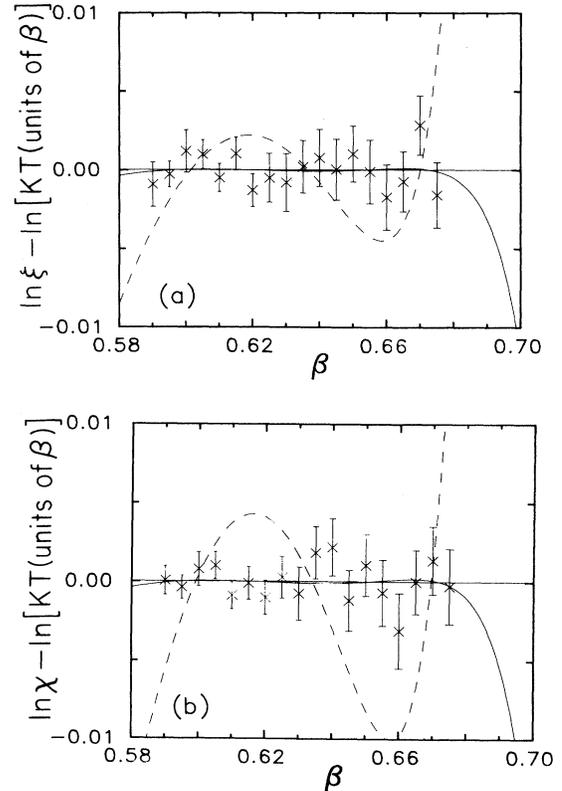
FIG. 11. (a) KT fits (continuous lines) and the β-dependent power-law fit (dashed line) to the correlation length data, using the β-dependent KT fit as a reference line. (b) The corresponding plot for the susceptibility.

strained KT fits with fixed $\nu = \frac{1}{2}$. As a result we obtain fits with reasonable goodness-of-fit parameters $Q > 0.2$ (see Table V). According to the usual interpretation this would be sufficient support for the theoretical hypothesis. When compared with the unconstrained fits, however, this interpretation is by no means unambiguous. The point becomes more transparent by observing that the results for χ^2 and β_c given in Table V can be read off from the χ^2 level plots in Fig. 10 by drawing a horizontal line at $\nu = 0.5$ and locating the crossing points with the long axis of the error ellipses. This clearly shows that data and theoretical prediction are only barely consistent and explains the interrelation between unconstrained and constrained fits. For the susceptibility we have also tested the influence of the leading correction to the KT prediction $\chi \propto \xi^{2-\eta} \rightarrow \chi \propto t^{-1/16} \xi^{2-\eta}$.[25] We obtain slightly modified fit parameters but do not find a further improvement of the fits. In addition we have studied for all fits the influence of the lower bound $\xi_{min} \approx 10$ by discarding more and more data points with small ξ. As a general tendency we observe that the various fits become more consistent with each other, but since at the same time the statistical errors on the fit parameters increase it is difficult to draw a quantitative conclusion from this study.

The source of the problem discussed above is obviously systematic errors which indicate that we are still too far away from the critical point, so that corrections cannot be neglected. The numerical difficulty is that the KT fits do not signal this by a large χ^2. From Fig. 11 we can read off that even if the error bars are reduced by a factor of 10, we could not decide which KT fit is more trustworthy. Also, adding more measurements up to $\beta = 0.7$ with the present accuracy, say, would not help. But already this is extremely demanding, since the correlation length at $\beta = 0.7$ is roughly 770, thus requiring lattice sizes $L > 4500$ for a reliable simulation.

C. Exponent η

The exponent η can be estimated from the high-temperature data in Tables I and II by means of the second KT relation in Eq. (1). In Fig. 12(a) we test the theoretical prediction $\eta = \frac{1}{4}$ by plotting $\ln(\chi / \xi^{7/4})$ versus $\ln \xi$. In such a plot a possible deviation $\Delta \eta \equiv \eta - \frac{1}{4}$ would show up as a straight line with slope $-\Delta \eta$. The data in Fig. 12(a) do not support this possibility, but follow a curved line with decreasing slope as ξ increases. This observation is depicted more quantitatively in Fig. 12(b) by plotting directly the local slopes of the curve in Fig. 12(a) (apart from an upward shift by $\frac{1}{4}$) which may be interpreted as effective exponents

$$\eta_i^{eff} \equiv 2 - \ln(\chi_{i+1}/\chi_{i-1})/\ln(\xi_{i+1}/\xi_{i-1}) \; , \tag{55}$$

with $\xi_i \equiv \xi(\beta_i)$, etc. From the point closest to criticality (corresponding to $\xi \approx 110-140$) we read off the estimate

$$\eta \approx \eta^{eff} \approx 0.267 \; , \tag{56}$$

which is still about 7% above the KT prediction. The slight downward tendency of η^{eff} may again be taken as
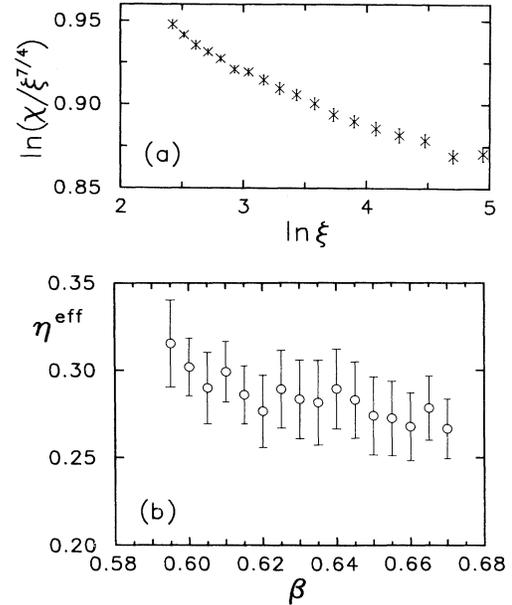
FIG. 12. Test of the KT prediction $\chi \propto \xi^{2-\eta}$ with $\eta = \frac{1}{4}$. The effective exponent in (b) is defined by the local slopes of the curve in (a) [see the text and Eq. (55)].

an indication that the asymptotic critical behavior sets in only in the very vicinity of the transition point.

VI. RESULTS AT CRITICALITY

In order to investigate this question further we have performed a second set of simulations near the transition point, i.e., deep inside the finite-size-scaling region. Our results at $\beta = 0.73, 0.74$, and 0.75 for lattices of sizes up to $L = 512$ are collected in Table VI. Energy and specific heat are almost insensitive to variations of L, and since the autocorrelation times for the susceptibility on the usual Metropolis scale become even smaller with increasing lattice size, there is certainly no critical slowing down using the single-cluster dynamics. The autocorrelation times for $g(x)$ behave similarly with a shallow minimum around $x \approx L/4$. For an illustration see Fig. 13.

In the following we shall concentrate on the susceptibility which, for large L and $\beta < \beta_c$, should obey the usual finite-size-scaling relation

$$\chi = L^{2-\eta} f(L / \xi_\infty) \; , \tag{57}$$

where ξ_∞ is the infinite volume limit of the correlation length. The scaling function $f(x)$ is expected to have the limiting behavior $f(x) \rightarrow a + bx + \cdots$ as $x \equiv L / \xi_\infty \rightarrow 0$ and $f(x) \rightarrow cx^{\eta-2}$ as $x \rightarrow \infty$ (a, b, c are constants). In the low-temperature phase for all $\beta \geq \beta_c$, the correlation length diverges, $\xi_\infty = \infty$, so that $x = 0$ and f is a constant independent of L and β. In this case finite-size scaling predicts that η has to be replaced by $\eta(\beta)$, where $\eta(\beta)$ is a decreasing function of β satisfying $\eta(\beta_c) \equiv \eta$. Extrapolating our KT fits in the high-temperature phase to $\beta = 0.73$, we estimate $\xi_\infty \approx 100\,000 - 180\,000$, implying

TABLE VI. Finite-size-scaling behavior near the transition point. For $L \leq 256$ measurements are taken every second, for $L=512$ every fourth cluster step.

β	L	$t_{run}/10^3$	f	χ	$\chi/L^{1.75}$	τ_χ	e	C_v
0.73	32	2278.8	0.6687	422.158(67)	0.980 53(16)	1.404(6)	0.726 850(56)	0.7652(11)
	64	394.0	0.5605	1 415.97(52)	0.977 78(36)	1.267(12)	0.727 909(68)	0.7711(27)
	100	616.6	0.4993	3 081.24(87)	0.974 37(28)	1.196(9)	0.728 278(36)	0.7761(22)
	128	362.6	0.4691	4 739.6(1.8)	0.973 03(36)	1.168(11)	0.728 378(37)	0.7749(27)
	200	109.8	0.4170	10 293.9(6.6)	0.967 78(63)	1.105(18)	0.728 430(43)	0.7775(51)
	256	62.8	0.3911	15 806(14)	0.964 69(81)	1.060(22)	0.728 482(44)	0.7864(67)
	512	43.3	0.6488	52 542(53)	0.953 42(95)	0.992(24)	0.728 486(28)	0.7793(82)
0.74	32	6953.6	0.6825	430.620(38)	1.000 188(89)	1.428(4)	0.712 894(31)	0.74025(62)
	64	484.5	0.5748	1 453.47(46)	1.003 67(32)	1.303(11)	0.713 997(60)	0.7458(23)
	100	526.2	0.5157	3 181.50(95)	1.006 08(30)	1.253(10)	0.714 240(37)	0.7478(22)
	128	531.4	0.4853	4 902.2(1.4)	1.006 40(29)	1.195(9)	0.714 251(29)	0.7431(22)
	200	116.1	0.4338	10 715.4(6.5)	1.007 41(61)	1.131(18)	0.714 342(39)	0.7412(46)
	256	84.1	0.4087	16 491(12)	1.006 54(70)	1.102(20)	0.714 358(37)	0.7537(56)
	512	29.2	0.6857	55 438(64)	1.006 0(12)	1.026(31)	0.714 337(33)	0.746(11)
0.75	32	1924.1	0.6955	438.638(72)	1.018 81(17)	1.455(7)	0.699 848(58)	0.7179(11)
	64	486.6	0.5888	1 489.06(46)	1.028 25(32)	1.351(12)	0.700 732(59)	0.7194(22)
	100	531.4	0.5297	3 269.15(93)	1.033 80(29)	1.256(10)	0.701 005(36)	0.7250(21)
	128	328.1	0.4997	5 048.4(1.8)	1.036 41(37)	1.232(12)	0.700 932(36)	0.7229(27)
	200	106.2	0.4500	11 077.2(6.7)	1.041 42(63)	1.168(20)	0.700 980(41)	0.7287(49)
	256	58.7	0.4230	17 109(14)	1.044 23(85)	1.171(26)	0.701 064(43)	0.7315(65)
	512	27.4	0.7142	58 001(67)	1.052 5(13)	1.086(35)	0.701 023(34)	0.7398(98)

that $x \leq 0.003-0.005$ is very small for all data points in Table VI. By plotting $\ln\chi$ versus $\ln L$ we obtain for all three temperatures apparently perfect straight lines with slope ≈ 1.75 as expected. Because of the very small error bars, however, only the goodness-of-fit parameter can indicate whether a linear fit is really acceptable, or alternatively we have to judge the data in a more sensitive plot. This is done in Fig. 14 where we plot $\chi/L^{1.75}$ versus L on a double logarithmic scale. For infinite correlation lengths we then expect straight lines with slope $\frac{1}{4} - \eta$, and for finite correlation lengths the data should be curved downward. This is clearly the case for $\beta=0.73$. At the two lower temperatures linear fits are justified for $L \geq 100$ and yield $\eta=0.2495\pm0.0006$ at $\beta=0.74$ (with $\chi^2=3.1$, $Q=0.38$), and $\eta=0.2389\pm0.0006$ at $\beta=0.75$ (with $\chi^2=0.19$, $Q=0.98$).

On the basis of its Q value the straight-line fit at $\beta=0.74$ appears acceptable. The value of η is consistent with the KT prediction $\eta=\frac{1}{4}$, but the corresponding estimate of $\beta_c \approx 0.74$ is lower than our earlier result (53) from fits to the high-temperature data $\beta_c \approx 0.75$. The discrepancy in the estimates of β_c suggests an alternative interpretation which, on purely numerical grounds, appears even more likely. When compared with the fit at $\beta=0.75$, the Q value at $\beta=0.74$ is relatively small. This observation may be taken as an indication that for $\beta=0.74$ the asymptotic finite-size-scaling region is not really reached up to $L=512$ and that the data could eventually curve downward for much larger lattice sizes, as is indeed visually suggested in Fig. 14. This is quite conceivable since the correlation length is very large near β_c. If we assume that on larger lattices the $\beta=0.75$ data

FIG. 13. Integrated autocorrelation times (rescaled to units of Metropolis sweeps) for the spatial correlation function $g(x)$ in the finite-size-scaling region.
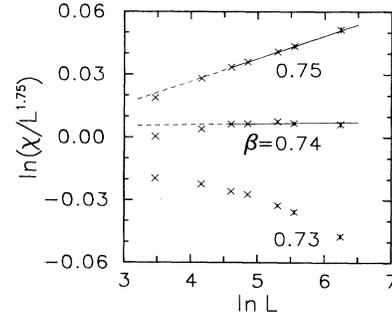
FIG. 14. Finite-size scaling of the susceptibility in the vicinity of the critical point, yielding the exponent η from linear fits for $L \geq 100$.

still follow the straight line in Fig. 14, this would imply that $\eta \approx 0.239 \neq \frac{1}{4}$ at $\beta_c \approx 0.75$, in disagreement with the KT prediction. It is interesting to note that Gupta and Baillie[21] found a similar value, $\eta \approx 0.235$, in their recent study of the cosine model.

Logically there is of course also the possibility that the $\beta = 0.75$ curve could become flatter on larger length scales and approach an asymptotic slope of zero. Since ξ_∞ is infinite at β_c, this would involve L-dependent corrections to scaling not taken into account in the ansatz (57). In view of the very good quality of the linear fit for $\beta = 0.75$, however, with the present data this possibility does not seem very plausible.

VII. CONCLUDING REMARKS

Our main result is that, among the two alternatives, a pure exponential or a pure power-law critical behavior, we find clear support for the exponential KT behavior in the two-dimensional XY Villain model. Estimates of the KT parameters from least-square fits to data in the high-temperature phase, however, turn out to be affected by rather large systematic errors which are difficult to control. Our results for the physically interesting parameters are $\beta_c = 0.752 \pm 0.005$ and $\nu = 0.48 \pm 0.10$.

From finite-size-scaling analyses of the second set of simulations in the vicinity of the critical point we obtain $\eta = 0.2495 \pm 0.0006 \approx \frac{1}{4}$ at $\beta = 0.74$ and $\eta = 0.2389 \pm 0.0006$ at $\beta = 0.75$. Relying on the estimate of β_c from the high-temperature data, we find a small but statistically significant deviation from the KT prediction $\eta = \frac{1}{4}$. It should be stressed, however, that this conclusion depends crucially on the precise value for β_c.

[1]N. D. Mermin and H. Wagner, Phys. Rev. Lett. **17**, 1133 (1966); P. C. Hohenberg, Phys. Rev. **158**, 383 (1967); N. D. Mermin, *ibid.* **176**, 250 (1968).

[2]H. E. Stanley and T. A. Kaplan, Phys. Rev. Lett. **17**, 913 (1966).

[3]J. M. Kosterlitz and D. J. Thouless, J. Phys. C **6**, 1181 (1973); V. L. Berezinskii, Zh. Eksp. Teor. Fiz. **61**, 1144 (1971) [Sov. Phys. JETP **34**, 610 (1972)].

[4]J. M. Kosterlitz, J. Phys. C **7**, 1046 (1974).

[5]For reviews, see P. Minnhagen, Rev. Mod. Phys. **59**, 1001 (1987); H. Kleinert, *Gauge Fields in Condensed Matter* (World Scientific, Singapore, 1989), Vol. I.

[6]J. Zittartz, Z. Phys. B **23**, 55, 63 (1976); A. Luther and D. J. Scalapino, Phys. Rev. B **16**, 1356 (1977); F. Fucito and S. Solomon, Phys. Lett. **134B**, 235 (1984).

[7]A. Patrascioiu and E. Seiler, Phys. Rev. Lett. **60**, 875 (1988); E. Seiler, I. O. Stamatescu, A. Patrascioiu, and V. Linke, Nucl. Phys. B **305**, 623 (1988).

[8]L. J. de Jongh and A. R. Miedema, Adv. Phys. **23**, 1 (1974).

[9]V. G. Vaks and A. I. Larkin, Zh. Eksp. Teor. Fiz. **49**, 975 (1965) [Sov. Phys. JETP **22**, 678 (1966)]; R. G. Bowers and G. S. Joyce, Phys. Rev. Lett. **19**, 630 (1967).

[10]E. Granato, J. M. Kosterlitz, and J. M. Lee, Phys. Rev. Lett. **66**, 1090 (1991); J. Lee, J. M. Kosterlitz, and E. Granato, Phys. Rev. B **43**, 11 531 (1991); A. Vallat and H. Beck, Phys. Rev. Lett. **68**, 3096 (1992); see also the articles in *Proceedings of the International Conference on Physics in Two Dimensions, Neuchatel, Switzerland, 1991* [Helv. Phys. Acta **65** (1992)].

[11]P. C. E. Stamp, L. Forro, and C. Ayache, Phys. Rev. B **38**, 2847 (1988); N.-C. Yeh and C. C. Tsuei, *ibid.* **39**, 9708 (1989); S. N. Artemenko, L. G. Gorlova, and Yu. I. Latyshev, Phys. Lett. A **138**, 428 (1989); J. Friedel, J. Phys. (Paris) **49**, 1561 (1988), J. Phys. Condens. Matter **1**, 7757 (1989).

[12]S. Martin, A. T. Fiory, R. M. Fleming, G. P. Espinosa, and A. S. Cooper, Phys. Rev. Lett. **62**, 677 (1989), **63**, 583 (1989).

[13]S. T. Chui and M. R. Giri, Phys. Lett. A **128**, 49 (1988); W.

Janke and T. Matsui, Phys. Rev. B **42**, 10673 (1990); P. Minnhagen and P. Olsson, Phys. Rev. Lett. **67**, 1039 (1991).

[14]W. Janke and K. Nather, in *Computer Simulation Studies in Condensed-Matter Physics V*, edited by D. P. Landau, K. K. Mon, and H.-B. Schüttler (Springer, Berlin, 1993); p. 140.

[15]P. Butera, M. Comi, and G. Marchesini, Phys. Rev. B **33**, 4725 (1986); **40**, 534 (1989).

[16]M. Ferer and Z. Mo, Phys. Rev. B **42**, 10769 (1990).

[17]P. Butera and M. Comi, Phys. Rev. B **47**, 11 969 (1993).

[18]R. Gupta, J. DeLapp, G. G. Battrouni, G. C. Fox, C. F. Baillie, and J. Apostolakis, Phys. Rev. Lett. **61**, 1996 (1988) (using an overrelaxation algorithm).

[19]U. Wolff, Nucl. Phys. B **322**, 759 (1989) (using the single-cluster update, but conventional observables).

[20]R. G. Edwards, J. Goodman, and A. D. Sokal, Nucl. Phys. B **354**, 289 (1991); A. Hulsebos, J. Smit, and J. C. Vink, *ibid.* **356**, 775 (1991) (using multigrid Monte Carlo simulations).

[21]R. Gupta and C. F. Baillie, Phys. Rev. B **45**, 2883 (1992).

[22]For earlier work using the Metropolis algorithm, see J. Tobochnik and G. V. Chester, Phys. Rev. B **20**, 3761 (1979); J. E. Van Himbergen and S. Chakravarty, *ibid.* **23**, 359 (1981); S. Samuel and F.-G. Yee, Nucl. Phys. B **257**, 85 (1985); P. Harten and S. Suranyi, *ibid.* **265**, 615 (1986); J. F. Fernández, M. F. Ferreira, and J. Stankiewicz, Phys. Rev. B **34**, 292 (1986).

[23]S. Ami and H. Kleinert, Phys. Rev. B **33**, 4692 (1986).

[24]J. V. José, L. P. Kadanoff, S. Kirkpatrick, and D. R. Nelson, Phys. Rev. B **16**, 1217 (1977); T. Ohta and K. Kawasaki, Prog. Theor. Phys. **60**, 365 (1978); L. Nakayama and T. Tsuneto, *ibid.* **63**, 402 (1980); J. L. Cardy and N. Parga, J. Phys. C **13**, 571 (1980).

[25]D. J. Amit, Y. Y. Goldschmidt, and G. Grinstein, J. Phys. A **13**, 585 (1980); L. P. Kadanoff and A. B. Zisook, Nucl. Phys. B **180**, 61 (1981).

[26]J. Villain, J. Phys. (Paris) **36**, 581 (1975).

[27]A brief account of some results of this section is already given in W. Janke and K. Nather, Phys. Lett. A **157**, 11 (1991).

[28]R. Savit, Rev. Mod. Phys. **52**, 453 (1980).

[29]Note that although Kosterlitz's (Ref. 4) analysis apparently starts from (4), his results actually apply to the periodic Gaussian model (5), as first noticed by Villain (Ref. 26).

[30]R. J. Myerson, Phys. Rev. B **16**, 3203 (1977).

[31]A. J. Guttmann (private communication).

[32]Y. Saito and H. Müller-Krumbhaar, Phys. Rev. B **23**, 308 (1981).

[33]W. Janke and H. Kleinert, Phys. Rev. B **41**, 6848 (1990). For earlier work, see also W. J. Shugard, J. D. Weeks, and G. H. Gilmer, Phys. Rev. Lett. **41**, 1399 (1978); **41**, 1577(E) (1978).

[34]N. Madras and A. D. Sokal, J. Stat. Phys. **50**, 109 (1988); A. D. Sokal, in *Quantum Fields on the Computer,* edited by M. Creutz (World Scientific, Singapore, 1992).

[35]R. H. Swendsen and J. S. Wang, Phys. Rev. Lett. **58**, 86 (1987); J.-S. Wang and R. H. Swendsen, Physica A **167**, 565 (1990).

[36]U. Wolff, Phys. Rev. Lett. **62**, 361 (1989).

[37]W. Janke, Phys. Lett. A **148**, 306 (1990).

[38]U. Wolff, Nucl. Phys. B **334**, 581 (1990).

[39]For more details, see K. Nather, Diploma-Thesis, Freie Universität Berlin, 1991.

[40]W. H. Press, B. P. Flannery, S. A. Teukolsky, and W. T. Vetterling, *Numerical Recipes—The Art of Scientific Computing* (Cambridge University Press, Cambridge, England, 1986).

[41]M. Hasenbusch, M. Marcu, and K. Pinn (unpublished).